

Recoil-Sensitive Lithium Interferometer without a Subrecoil Sample

Kayleigh Cassella,^{1,*} Eric Copenhaver,¹ Brian Estey,¹ Yanying Feng,² Chen Lai,³ and Holger Müller^{1,†}

¹*Department of Physics, 366 LeConte Hall, Berkeley, California 94720, USA*

²*Joint Institute for Measurement Science, State Key Laboratory of Precision Measurement Technology and Instruments, Department of Precision Instruments, Tsinghua University, Beijing 100084, China*

³*Department of Mathematics, University of California, San Diego, La Jolla, California 92093-0404, USA*

(Received 26 October 2016; published 9 June 2017)

We report simultaneous conjugate Ramsey-Bordé interferometers with a sample of low-mass (lithium-7) atoms at 50 times the recoil temperature. We optically pump the atoms to a magnetically insensitive state using the $2S_{1/2} - 2P_{1/2}$ line. Fast stimulated Raman beam splitters address a broad velocity class and unavoidably drive two conjugate interferometers that overlap spatially. We show that detecting the summed interference signals of both interferometers, using state labeling, allows recoil measurements and suppression of phase noise from vibrations. The use of “warm” atoms allows for simple, efficient, and high-flux atom sources and broadens the applicability of recoil-sensitive interferometry to particles that remain difficult to trap and cool.

DOI: 10.1103/PhysRevLett.118.233201

In a light-pulse atom interferometer, laser pulses with wave number k direct matter waves along a superposition of trajectories and recombine them to reveal the phase difference between paths [1]. They are used for inertial sensing [2,3], gravity gradiometry [4], and tests of fundamental physics [5–15]. Ramsey-Bordé interferometers, in particular, measure the mass m of an atom through the kinetic energy $\hbar\omega_r = \hbar^2 k^2 / (2m)$ it gains after recoiling from the interaction with a photon (\hbar is the reduced Planck constant). They can help redefine the kilogram [16,17] and determine the fine-structure constant [18–22], thereby testing the standard model [23,24]. The recoil frequency ω_r , and therefore the signal, scales inversely with mass. Light atomic species have been used in supersonic atomic-beam interferometers [25,26], but remain difficult to cool below the recoil temperature T_r , where the average thermal speed equals the recoil velocity. This makes it impossible to spatially resolve the interferometer outputs, which is required for direct rejection of common-mode inertial signals with phase extraction methods [27–29].

Here, we demonstrate recoil-sensitive interferometry with a sample of lithium-7 atoms well above the atomic recoil temperature ($50T_r$), the first interferometer with laser-cooled lithium atoms or any atom lighter than sodium-23 [30]. Fast Raman transitions [31] ($\tau_{\pi/2} = 160$ ns) address the ensemble’s large Doppler spread and simultaneously drive overlapped conjugate Ramsey-Bordé interferometers. Superimposing simultaneous conjugate interferometers suppresses effects from two-photon detuning and unwanted inertial signals, such as vibrations. Our measurement sensitivity benefits from lithium’s high recoil frequency of $\omega_r = 2\pi \times 63$ kHz (compared to $2\pi \times 2$ kHz for cesium) and the absence of time-consuming additional cooling [32] or lossy velocity

selection [33] steps that reduce sample size and precision. The lithium isotopes present an attractive pair for testing Einstein’s equivalence principle using light-pulse atom interferometry [34]. This work broadens the applicability of recoil-sensitive interferometry to other particles; electrons [35], for example, boast GHz-recoil frequencies and would enable observation of relativistic effects [16,36].

Figure 1(a) shows the trajectories of an atom in a Ramsey-Bordé sequence. Atom-light interactions are used to split, redirect, and interfere the atomic matter waves. The Ramsey-Bordé sequence consists of four $\pi/2$ (beam splitter) pulses, so that the lowest interferometer arm remains stationary. The outputs of the second pulse that do not contribute to A^- and B^- may form another conjugate (upper) interferometer with final outputs A^+ and B^+ .

In each interferometer, the probability of detecting the atoms at one output depends on the phase difference between the arms of the interferometer, which we denote $\Delta\phi^-$ ($\Delta\phi^+$) for the lower (upper) interferometer. Using standard methods [37], $\Delta\phi^\pm$ is calculated to second order in T as

$$\Delta\phi^\pm = \pm 8\omega_r T - 2ka_z T(T + T') - 2\delta T. \quad (1)$$

The first term arises from the atomic kinetic energy, the second from any acceleration a_z (such as gravity and vibrations) along the laser beam axis, where the average wave number of the counterpropagating beams is $k = (k_1 + k_2)/2$, and the third from the detuning of the laser frequencies from two-photon resonance in the absence of ac Stark shifts, $\delta = \omega_1 - \omega_2 - (\omega_A - \omega_B)$ [38].

The interferometers in Fig. 1(a) share the first and second beam splitter pulses. For the third and fourth pulses, the lower interferometer requires a transition coupling

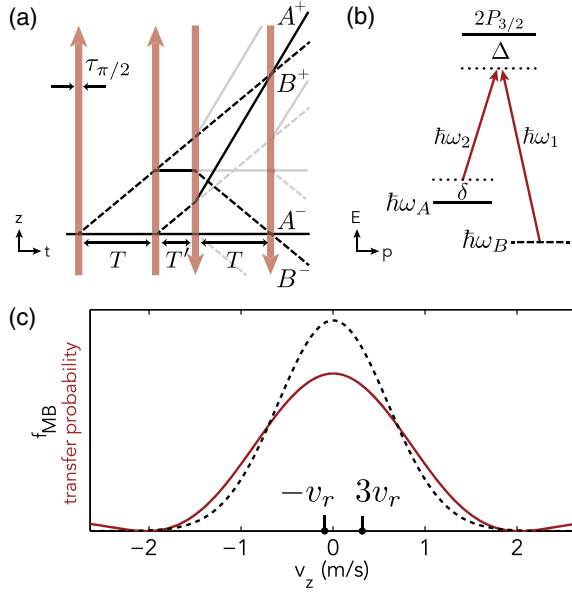


FIG. 1. Ramsey-Bordé interferometry with high temperatures: (a) Space-time trajectories of atoms in Ramsey-Bordé interferometers, neglecting gravity. Solid and dashed lines indicate internal states of the atom, for example, hyperfine ground states. Interfering trajectories are shown in black and noninterfering outputs are shown in light gray. Arrows on the light pulses represent the effective wave vector. (b) Energy levels and frequencies involved in Raman transitions. (c) The bandwidth of the atomic response to a $\pi/2$ pulse (solid red line) is inversely proportional to pulse duration, while the velocity width of the Maxwell-Boltzmann distribution along the Raman axis (dashed black line) is proportional to the square root of the temperature (here, $300 \mu\text{K}$). The 160-ns pulses cover a large velocity class, including the speeds that Doppler shift the third and fourth pulses onto resonance for each conjugate interferometer.

$|F = 2, p = 0\rangle \rightarrow |F = 1, p = -2\hbar k\rangle$, and the upper interferometer requires coupling $|F = 1, p = +2\hbar k\rangle \rightarrow |F = 2, p = +4\hbar k\rangle$. Reversing the effective wave vector of the beam splitters for the second pulse pair accomplishes both of these couplings. In principle, they are distinguished by a Doppler shift of $8\omega_r$ due to the speed difference between the lower and upper interferometer, as marked in Fig. 1(c). Low-bandwidth beam splitter pulses for atom interferometers typically resolve this frequency difference, but the high-bandwidth pulses we use to address a broad velocity class simultaneously address both transitions, unavoidably closing both interferometers. The two interferometers' outputs ports (e.g., B^- , B^+) overlap spatially since the samples thermally expand faster than the interferometers separate.

We recover the recoil signal by using Raman beam splitters, which allow us to use state-dependent detection of the sum of signals from the lower and upper interferometers. Beginning in the $|F = 2\rangle$ ground state (state A) prior to the interferometry pulse sequence, the probability for an atom to emerge from the interferometer in the $|F = 1\rangle$ ground state (state B) oscillates as

$$P_B = D[1 - C_- \cos(\Delta\phi^-) - C_+ \cos(\Delta\phi^+)], \quad (2)$$

where C_{\pm} are the fringe contrasts of each interferometer and D is an overall offset. For approximately equal contrasts, $C_+ = C_- \equiv C/2$, the signal simplifies to

$$P_B = D\{1 - C \cos[2ka_z T(T+T') + 2\delta T] \cos(8\omega_r T)\}. \quad (3)$$

Our setup is similar to the one previously described in Ref. [39] but without the polarization gradient lattice used for sub-Doppler cooling. We heat lithium to 400°C and trap the vapor in a two-dimensional magneto-optical trap (MOT). A push beam tuned near resonance sends the atoms through a differential pumping tube into the interferometry chamber, where approximately 15×10^6 atoms are trapped in a three-dimensional MOT. After lowering the intensities of both the cooling and repumping light and moving the detuning closer to resonance, the cloud reaches a final temperature of roughly $300 \mu\text{K}$.

To define a quantization axis for optical pumping and Raman transitions, we apply a bias magnetic field of 1 G along the \hat{z} axis. Despite the $250\text{-}\mu\text{s}$ decay of the current in the anti-Helmholtz MOT coils, the quadrupole field remains appreciable for milliseconds due to eddy currents in the steel vacuum chamber. We use the 3D MOT beams as optical molasses to limit the thermal expansion of the cloud while the eddy currents decay. No polarization gradient cooling occurs during this step due to the small detuning of the 3D MOT beams from the unresolved D_2 line ($2P_{3/2}$ state) [39].

After the optical molasses, the atoms are distributed among the five nondegenerate magnetic sublevels of the $|F = 2\rangle$ ground-state manifold. This leads to magnetic dephasing since the Ramsey-Bordé interferometer phase depends on the internal energies through the δ term. Interferometer experiments often select atoms in the desired magnetic sublevel by transferring them to the other hyperfine state with a microwave and blowing away the remaining populations with resonant light. The unresolved D_2 line in lithium, however, precludes the efficient cycling transitions required to impart the large momentum needed for such blow-away beams. Furthermore, this selection process is lossy, as large atomic populations are sacrificed to the blow-away beam.

To avoid the magnetic dephasing from atoms in different magnetic sublevels, we optically pump the sample to the magnetically insensitive $|F = 2, m_F = 0\rangle$ state by taking advantage of the selection rule that prohibits $m_F = m'_F = 0$ transitions when $\Delta F = 0$. Once the magnetic field gradient decays below 1 G/cm (after 1.5 ms of optical molasses), we send 3 mW of light tuned within a linewidth ($\Gamma/2\pi = 5.87$ MHz) of the $|F = 2\rangle$ to $|F' = 2\rangle$ transition on the well-resolved D_1 line ($2P_{1/2}$ state). The optical pumping light is π polarized along \hat{z} and has a 3.6-mm Gaussian waist. Unlike the D_2 line, lithium's D_1 line has a resolved hyperfine structure [see Fig. 2(b)]. Optical pumping on the D_1 line therefore avoids the slightly off-resonant transitions ubiquitous on the D_2 line [40]. In each of the six

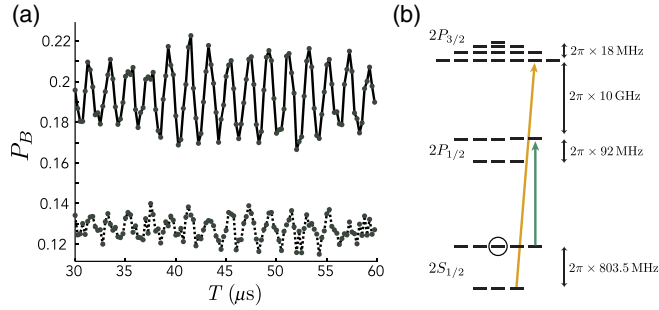


FIG. 2. Optical pumping. (a) Interference fringes without optical pumping (lower dashed curve) and with optical pumping (upper solid curve). Each gray point on the traces is the average of five experimental shots, and error bars are omitted for clarity. (b) Optical pumping on lithium's D_1 line with π light (green arrow) results in a dark state at $|F = 2, m_F = 0\rangle$ (black circle). Atoms that decay to $|F = 1\rangle$ are recovered by 3D MOT repump light (yellow arrow). Each dash represents a unique magnetic sublevel.

3D MOT beams, we use 1.5 mW of D_2 MOT repump light to recover atoms that decay to $|F = 1\rangle$. We tune the repump frequency closer to resonance, optimizing for optical pumping efficiency. After $50 \mu\text{s}$ of optical pumping, more than 80% of the atoms occupy the dark state.

Figure 2 displays the efficacy of the optical pumping for interferometry. Without optical pumping, the recoil fringes have low contrast, a low signal-to-noise ratio, and decohere more rapidly, limiting the maximum interrogation time and sensitivity. Preparation to the magnetically insensitive $|F = 2, m_F = 0\rangle$ state before interferometry increases the contrast and signal-to-noise ratio by more than a factor of 2 at short interrogation times. Optical pumping also makes the fringes visible at longer interrogation times.

After optical pumping, we measure the fringes by varying the separation time T while keeping $T' = 10 \mu\text{s}$ and δ constant but small compared to ω_r . To close the interferometers, we reverse the direction of the Raman beams for the second pulse pair using an electro-optic modulator (see Supplemental Material [41]). For normalized detection, we use a new imaging technique that captures two images during a single exposure (see Supplemental Material [41]).

Figure 3 shows the summed interference fringes obtained from the simultaneous conjugate Ramsey-Bordé interferometers. As seen in Eq. (3), they can be described by a fast oscillation at a frequency of $8\omega_r$ within an envelope function that oscillates slowly at a frequency set by the two-photon detuning 2δ , in addition to accelerations a_z . Here, the two-photon detuning term dominates over phases induced by acceleration because we operate our interferometer perpendicular to gravity and at short interrogation times. Figure 3(b) shows the fast component of the summed fringes. We fit the fringes using a least-squares method to the functional form in Fig. 3(b). The confidence interval in the fit constitutes a 32-ppm recoil measurement in 2 h. After averaging across 10 such data sets with varying

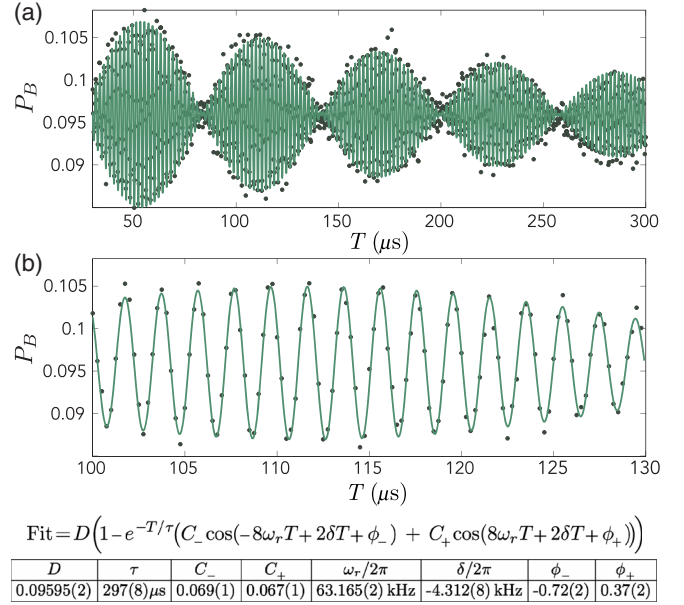


FIG. 3. Beating interference of overlapped interferometers. (a) The probability of detecting atoms in the $|F = 1\rangle$ state oscillates, beating due to a nonzero $\delta = -2\pi \times 4.3$ kHz. Each point is the average of five experimental shots with error bars omitted for clarity. Fitting (in green) yields $\omega_r = 2\pi \times (63.165 \pm 0.002)$ kHz). (b) Closer inspection reveals the fast recoil component of the fringes. The table at the bottom shows results of the fit with 1σ precision.

δ , we reached a precision of 10 ppm. The phase sensitivity of the fit corresponds to a sensitivity roughly 50 times larger than the shot-noise limit.

The noise observed in the data is due mostly to laser noise, as we have confirmed by numerical simulations adapted from previous studies of noise in Ramsey-Bordé interferometers [42]. The linewidth of the Raman laser ($\gamma/2\pi \approx 1$ MHz) is sizable compared to the small magnitude of the single-photon detuning ($\Delta/2\pi = 210$ MHz) and creates pulse-to-pulse fluctuations of the two-photon Rabi frequency, which result in noise significantly larger than the shot-noise-limited sensitivity.

The coherence time of the interferometer is not yet limited by thermal expansion out of the Raman beam but instead by magnetic dephasing of the $m_F = 0$ atoms. The magnetic field gradient that survives after the optical molasses gives rise to inhomogeneous quadratic Zeeman shifts, leading to an interferometer phase dependent on an atom's position in the cloud. We are able to reduce the magnetic gradient by extending the optical molasses time to 5 ms and, with half the remaining gradient, the interference contrast indeed decays at half the rate. Magnetic gradient compensation would lead to longer coherence times and improved sensitivity. At a conservatively projected $T = 1$ ms, we estimate the shot-noise-limited sensitivity with 10^7 atoms to be $100 \text{ ppb}/\sqrt{\text{Hz}}$. Implementing sub-Doppler cooling techniques [39,43] to reach a temperature of $40 \mu\text{K}$ (approximately $8T_r$) would improve the

sensitivity by $\sqrt{50/8} \sim 3$, but still require the techniques in this Letter.

Phase shifts due to vibrations cancel when the fringes are summed in our detection scheme, as they enter the conjugate interferometers with opposite sign. The only effect of vibrations is then an amplitude modulation of the fringes. Consider Eq. (1) with a stochastic, Gaussian-distributed a_z with 0 mean and standard deviation σ . When $2k\sigma T(T + T') \ll \pi$, the effect of such vibrations is a modulation of the interference contrast, which decreases proportionally to a_z^2 . Other interferometers operating on a similar optical table without vibration isolation accrue phase shifts much less than π due to vibrations, even at $T = 10$ ms [15]. Lithium's high recoil frequency allows us to take sensitive data at $T < 10$ ms, and therefore to make full use of the common-mode rejection of vibration-induced signals.

This demonstration of interferometry opens the door to recoil measurements with other particles that are difficult to cool to subrecoil temperatures, such as electrons. Electrons, whose recoil frequency is on the order of GHz, are susceptible to relativistic effects, and consequently, a recoil-sensitive measurement can be used to measure Lorentz contraction [36]. While Kapitza-Dirac scattering has been proposed to realize matter-wave beam splitters for electrons in a Ramsey-Bordé interferometer [44], any vibrations or nonzero two-photon detuning will modify the phase ($\Delta\phi^-$) for a single Ramsey-Bordé. As we have shown in this work, the inclusion of the simultaneous conjugate interferometer ($\Delta\phi^+$) recovers the recoil phase independently of a two-photon detuning even when the outputs of conjugate interferometers are spatially unresolved, as would be the case for electron plasmas in a Penning-Malmberg trap [35]. The required spectral resolution for detection could be achieved with bichromatic Kapitza-Dirac pulses. Bichromatic pulses with very large intensity have been proposed to impart momentum to an electron while inducing a spin flip [45] and hence couple the electron's external and internal degrees of freedom. With such beam splitters acting on a spin-polarized sample and spin-dependent detection, the techniques we demonstrate in this work pave the way for a recoil-sensitive electron interferometer.

In summary, we demonstrate recoil-sensitive Ramsey-Bordé interferometry with laser-cooled lithium-7 at 300 μ K ($50T_r$). The large Doppler spread of the sample is addressed with fast pulses, driving simultaneous conjugate interferometers with nearly equal contrast. Even with nonzero two-photon detuning, the interference fringes allow for the determination of the recoil frequency independent of two-photon detuning and vibrations. We suppress first-order magnetic dephasing and extend the coherence time by optically pumping the atoms to the magnetically insensitive $|F = 2, m_F = 0\rangle$ state using lithium-7's well-resolved D_1 line. Our results relax cooling requirements for recoil interferometry, allowing for

increased precision through high experimental repetition rates [31,46]. Extending these techniques would allow for recoil-sensitive interferometry with atoms and other particles that have thus far been excluded from such experiments.

We thank Paul Hamilton, Philipp Haslinger, Matt Jaffe, Geena Kim, Richard Parker, Simon Budker, Quinn Simmons, Dennis Schlippert, and Daniel Tiarks for help with the experiment and discussions. This material is based upon work supported by the National Science Foundation under Grant No. 031510 and by the David and Lucile Packard Foundation.

*kcassell@berkeley.edu

†Present address: Molecular Biophysics and Integrated Bioimaging, Lawrence Berkeley National Laboratory, 1 Cyclotron Road, Berkeley, California 94720, USA.

- [1] A. D. Cronin, J. Schmiedemayer, and D. E. Pritchard, Optics and interferometry with atoms and molecules, *Rev. Mod. Phys.* **81**, 1051 (2009).
- [2] A. Peters, K.-Y. Chung, and S. Chu, Measurement of gravitational acceleration by dropping atoms, *Nature (London)* **400**, 849 (1999).
- [3] R. Geiger, V. Ménotet, G. Stern, N. Zahzam, P. Cheinet, B. Battelier, A. Villing, F. Moron, M. Lours, Y. Bidel, A. Bresson, A. Landragin, and P. Bouyer, Detecting inertial effects with airborne matter-wave interferometry, *Nat. Commun.* **2**, 474 (2011).
- [4] J. M. McGuirk, G. T. Foster, J. B. Fixler, M. J. Snadden, and M. A. Kasevich, Sensitive absolute-gravity gradiometry using atom interferometry, *Phys. Rev. A* **65**, 033608 (2002).
- [5] G. Rosi, F. Sorrentino, F. Cacciapuoti, and M. Prevedelli, Precision measurement of the Newtonian gravitational constant using cold atoms, *Nature (London)* **510**, 518 (2014).
- [6] K.-Y. Chung, S.-w. Chiow, S. Herrmann, S. Chu, and H. Müller, Atom interferometry tests of local Lorentz invariance in gravity and electrodynamics, *Phys. Rev. D* **80**, 016002 (2009).
- [7] M. A. Hohensee, B. Estey, P. Hamilton, A. Zeilinger, and H. Müller, Force-Free Gravitational Redshift: Proposed Gravitational Aharonov-Bohm Experiment, *Phys. Rev. Lett.* **108**, 230404 (2012).
- [8] S. Fray, C. A. Diez, T. W. Hänsch, and M. Weitz, Atomic Interferometer with Amplitude Gratings of Light and Its Applications to Atom Based Tests of the Equivalence Principle, *Phys. Rev. Lett.* **93**, 240404 (2004).
- [9] H. Müller, A. Peters, and S. Chu, A precision measurement of the gravitational redshift by the interference of matter waves, *Nature (London)* **463**, 926 (2010).
- [10] A. Bonnin, N. Zahzam, Y. Bidel, and A. Bresson, Simultaneous dual-species matter-wave accelerometer, *Phys. Rev. A* **88**, 043615 (2013).
- [11] D. Schlippert, J. Hartwig, H. Albers, L. L. Richardson, C. Schubert, A. Roura, W. P. Schleich, W. Ertmer, and E. M. Rasel, Quantum Test of the Universality of Free Fall, *Phys. Rev. Lett.* **112**, 203002 (2014).

- [12] M. G. Tarallo, T. Mazzoni, N. Poli, D. V. Sutyryn, X. Zhang, and G. M. Tino, Test of Einstein Equivalence Principle for 0-Spin and Half-Integer-Spin Atoms: Search for Spin-Gravity Coupling Effects, *Phys. Rev. Lett.* **113**, 023005 (2014).
- [13] L. Zhou, S. Long, B. Tang, X. Chen, F. Gao, W. Peng, W. Duan, J. Zhong, Z. Xiong, J. Wang, Y. Zhang, and M. Zhan, Test of Equivalence Principle at 10^{-8} Level by a Dual-Species Double-Diffraction Raman Atom Interferometer, *Phys. Rev. Lett.* **115**, 013004 (2015).
- [14] X.-C. Duan, X.-B. Deng, M.-K. Zhou, K. Zhang, W.-J. Xu, F. Xiong, Y.-Y. Xu, C.-G. Shao, J. Luo, and Z.-K. Hu, Test of the Universality of Free Fall with Atoms in Different Spin Orientations, *Phys. Rev. Lett.* **117**, 023001 (2016).
- [15] P. Hamilton, M. Jaffé, P. Haslinger, Q. Simmons, H. Müller, and J. Khoury, Atom-interferometry constraints on dark energy, *Science* **349**, 849 (2015).
- [16] S.-Y. Lan, P.-C. Kuan, B. Estey, D. English, J. Brown, M. Hohensee, and H. Müller, A clock directly linking time to a particle's mass, *Science* **339**, 554 (2013).
- [17] R. Bouchendira, P. Cladé, S. Guellati-Khélifa, F. Nez, and F. Biraben, State of the art in the determination of the fine structure constant: test of Quantum Electrodynamics and determination of h/m_e , *Ann. Phys. (Berlin)* **525**, 484 (2013).
- [18] D. S. Weiss, B. C. Young, and S. Chu, Precision measurement of \hbar/m_{Cs} based on photon recoil using laser-cooled atoms and atomic interferometry, *Appl. Phys. B* **59**, 217 (1994).
- [19] A. Wicht, J. M. Hensley, E. Sarajlic, and S. Chu, A preliminary measurement of the fine structure constant based on atom interferometry, *Phys. Scr.* **T102**, 82 (1999).
- [20] R. Bouchendira, P. Clade, S. Guellati-Khelifa, F. Nez, and F. Biraben, New Determination of the Fine Structure Constant and Test of the Quantum Electrodynamics, *Phys. Rev. Lett.* **106**, 080801 (2011).
- [21] A. O. Jamison, B. Plotkin-Swing, and S. Gupta, Advances in precision contrast interferometry with Yb Bose-Einstein condensates, *Phys. Rev. A* **90**, 063606 (2014).
- [22] B. Estey, C. Yu, H. Müller, P.-C. Kuan, and S.-Y. Lan, High-Resolution Atom Interferometers with Suppressed Diffraction Phases, *Phys. Rev. Lett.* **115**, 083002 (2015).
- [23] G. Gabrielse, D. Hanneke, T. Kinoshita, M. Nio, and B. Odom, New Determination of the Fine Structure Constant from the Electron g Value and QED, *Phys. Rev. Lett.* **97**, 030802 (2006).
- [24] Y. Ding and V. A. Kostelecky, Lorentz-violating spinor electrodynamics and Penning traps, *Phys. Rev. D* **94**, 056008 (2016).
- [25] C. Champenois, M. Büchner, and J. Vigué, Fringe contrast in three grating Mach-Zehnder atomic interferometers, *Eur. Phys. J. D* **5**, 363 (1999).
- [26] M. Jacquy, M. Büchner, G. Tréneç, and J. Vigué, First measurements of the index of refraction of gases for lithium atomic waves, *Phys. Rev. Lett.* **98**, 240405 (2007).
- [27] S.-w. Chiow, S. Herrmann, S. Chu, and H. Müller, Noise-Immune Conjugate Large-Area Atom Interferometers, *Phys. Rev. Lett.* **103**, 050402 (2009).
- [28] S.-w. Chiow, J. Williams, and N. Yu, Noise reduction in differential phase extraction of dual atom interferometers using an active servo loop, *Phys. Rev. A* **93**, 013602 (2016).
- [29] J. K. Stockton, X. Wu, and M. A. Kasevich, Bayesian estimation of differential interferometer phase, *Phys. Rev. A* **76**, 033613 (2007).
- [30] M. Kasevich and S. Chu, Atomic Interferometry Using Stimulated Raman Transitions, *Phys. Rev. Lett.* **67**, 181 (1991).
- [31] G. W. Biedermann, H. J. McGuinness, A. V. Rakholia, Y.-Y. Jau, D. R. Wheeler, J. D. Sterk, and G. R. Burns, Atom Interferometry in a Warm Vapor, *Phys. Rev. Lett.* **118**, 163601 (2017).
- [32] P. M. Duarte, R. A. Hart, J. M. Hitchcock, T. A. Corcovilos, T.-L. Yang, A. Reed, and R. G. Hulet, All-optical production of a lithium quantum gas using narrow-line laser cooling, *Phys. Rev. A* **84**, 061406 (2011).
- [33] M. Kasevich, D. S. Weiss, E. Riis, K. Moler, S. Kasapi, and S. Chu, Atomic Velocity Selection Using Stimulated Raman Transitions, *Phys. Rev. Lett.* **66**, 2297 (1991).
- [34] M. A. Hohensee, H. Müller, and R. B. Wuringa, Equivalence Principle and Bound Kinetic Energy, *Phys. Rev. Lett.* **111**, 151102 (2013).
- [35] A. P. Povilus, N. D. DeTal, L. T. Evans, N. Evetts, J. Fajans, W. N. Hardy, E. D. Hunter, I. Martens, F. Robicheaux, S. Shanman, C. So, X. Wang, and J. S. Wurtele, Electron Plasmas Cooled by Cyclotron-Cavity Resonance, *Phys. Rev. Lett.* **117**, 175001 (2016).
- [36] K.-P. Marzlin and T. Lee, Interferometry with relativistic electrons, *Phys. Rev. A* **89**, 062103 (2014).
- [37] J. M. Hogan, D. M. S. Johnson, and M. A. Kasevich, Light-pulse atom interferometry, [arXiv:0806.3261](https://arxiv.org/abs/0806.3261).
- [38] We call this term a two-photon detuning loosely. It is the difference between the Raman laser frequency difference $\omega_1 - \omega_2$ and the hyperfine splitting $\omega_A - \omega_B$ during free evolution [see Fig. 1(b)]. That is, our so-called two-photon detuning does not include ac Stark shifts of the internal hyperfine energies induced when the Raman light dresses the atoms, but it does include other shifts that persist during free evolution, such as Zeeman shifts.
- [39] P. Hamilton, G. Kim, T. Joshi, B. Mukherjee, D. Tiarks, and H. Müller, Sisyphus cooling of lithium, *Phys. Rev. A* **89**, 023409 (2014).
- [40] J. Gillot, A. Gauguet, M. Büchner, and J. Vigué, Optical pumping of a lithium atomic beam for atom interferometry, *Eur. Phys. J. D* **67**, 263 (2013).
- [41] See Supplemental Material at <http://link.aps.org/supplemental/10.1103/PhysRevLett.118.233201> for more experimental details.
- [42] R. H. Parker, C. Yu, B. Estey, W. Zhong, E. Huang, and H. Müller, Controlling the multiport nature of Bragg diffraction in atom interferometry, *Phys. Rev. A* **94**, 053618 (2016).
- [43] A. T. Grier, I. Ferrier-Barbut, B. S. Rem, M. Delehay, L. Khaykovich, F. Chevy, and C. Salomon, Λ -enhanced sub-Doppler cooling of lithium atoms in D_1 gray molasses, *Phys. Rev. A* **87**, 063411 (2013).
- [44] K.-P. Marzlin, Ramsey-Bordé interferometer for electrons, *Phys. Rev. A* **88**, 043621 (2013).
- [45] S. McGregor, W. C.-W. Huang, B. A. Shadwick, and H. Batelaan, Spin-dependent two-color Kapitza-Dirac effects, *Phys. Rev. A* **92**, 023834 (2015).
- [46] A. V. Rakholia, H. J. McGuinness, and G. W. Biedermann, Dual-Axis High-Data-Rate Atom Interferometer via Cold Ensemble Exchange, *Phys. Rev. Applied* **2**, 054012 (2014).